

Improving Adaptability and Generalizability of Efficient Transfer Learning for Vision-Language Models

Yongjin Yang* Jongwoo Ko* Se-Young Yun

KAIST AI

{dyyjkd, jongwoo.ko, yunseyoung}@kaist.ac.kr

Abstract

Vision-Language Models (VLMs) like CLIP have demonstrated remarkable applicability across a variety of downstream tasks, including zero-shot image classification. Recently, the use of prompts or adapters for efficient transfer learning has gained significant attention for effectively adapting to downstream tasks. However, the roles of vision and text prompts, as well as adapters in terms of generalization and transfer difficulty, have been overlooked, limiting performance on unseen tasks. In this paper, we empirically analyze how VLMs behave when using vision and text prompts, adapters, and a combination of these components, marking a novel exploration by our study. Our observations find that utilizing vision prompts for class separability and text adapters for task adaptation is crucial for adaptability and generalizability. Moreover, to improve generalization across every domain, we propose an adaptive ensemble method that effectively combines the general knowledge of VLMs with task-specific knowledge according to transfer difficulty. Upon experimenting with extensive benchmarks, our method consistently outperforms all baselines, particularly on unseen tasks, demonstrating the effectiveness of our proposed approach.

1. Introduction

Vision-language models (VLMs), such as CLIP [32] and ALIGN [14], have demonstrated remarkable applicability across various downstream tasks such as image classification. A distinctive feature of these VLMs for image classification is their ability to classify novel classes that have not been encountered during pre-training through zero-shot inference. To boost this ability, recent research has introduced efficient transfer learning (ETL) methods to fine-tune VLMs. One strategy involves the use of soft prompt tuning [16, 17, 47, 48]. Another research direction involves adapter-style tuning [8, 46, 50] either by adjusting specific parameters or employing cache-based techniques. These ap-

proaches empower VLMs to swiftly adapt to new tasks using only a few samples (i.e. few-shot image classification task).

However, previous research on ETL has overlooked the importance of configuring prompt and adapter-style tuning methods to enhance generalizability, thereby limiting performance on tasks that are not seen during few-shot adaptation. Furthermore, previous studies have not considered transfer difficulty, which is the challenge of adapting pretrained VLMs, according to the target domain. For instance, transferring pre-trained VLMs to specific fine-grained domains, like FGVC Aircraft, is more challenging than to general coarse-grained domains. In general, domains with high transfer difficulty demand a greater amount of task-specific information compared to those with low difficulty. Failure to consider this leads to suboptimal adaptation to the target domain.

In this paper, we empirically investigate the characteristics of each encoder of different modalities and tuning methods, revealing four key findings related to generalizability and transfer difficulty. *Firstly*, we find that visual prompt tuning (VPT) better generalizes to unseen classes compared to text prompt tuning (TPT) (\triangleright Obs. 1). On the other hand, while TPT performs better with seen classes, it tends to overfit to these classes, particularly in cases of high transfer difficulty. This occurs because in high-difficulty domains, the class separability of visual features from a visual encoder is low, causing TPT to overly adapt in classifying these challenging features (\triangleright Obs. 2). *Moreover*, text adapter (TA) can complement the low adaptation capabilities of VPT, resulting in an overall adaptation comparable to TPT while minimizing overfitting and thus boosting the performance on difficult domains (\triangleright Obs. 3). *Finally*, by modulating the impact of TA through an ensemble of pre-adapters and post-adapters with varying coefficients, we can enhance performance in domains with low difficulty while maintaining effectiveness in difficult domains (\triangleright Obs. 4). Therefore, estimating the transfer difficulty to calculate the domain-adaptive coefficient for ensemble can boost adaptability and generalizability across all domains by properly utilizing both general and task-specific knowledge, as illustrated in Figure 1(b).

Based on our observations, we present a **APEX** (text

* equal contribution

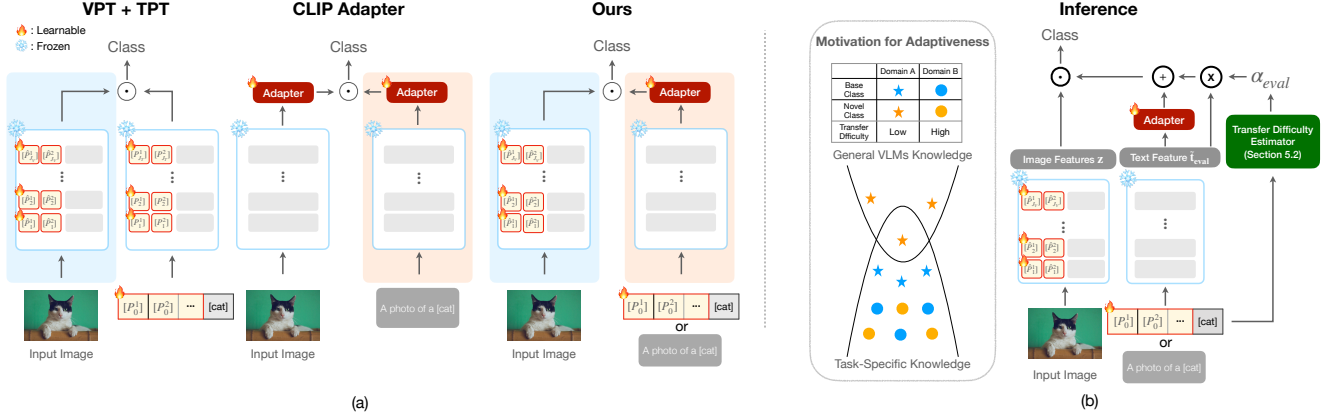


Figure 1. Overview of our **APEX** compared to the conventional efficient transfer learning methods. **APEX** exhibits two key differences: (a): Firstly, **APEX** integrates prompt tuning for the visual encoder and a linear adapter for the text encoder, each tailored to the specific properties of their respective modalities, as identified in our observations. (b): Secondly, **APEX** integrates an adaptive coefficient within the text encoder to strategically balance pre-adapter and post-adapter features to properly combine task-specific knowledge and general VLMs knowledge. A detailed explanation, including notations and the algorithm, can be found in Section 5 and the Appendix B.

Adapter, visual **Prompt**, and adaptive **Ensemble** for cross(X)-modality) that incorporates the VPT, TA, along with an adaptive ensemble approach used for evaluation. Specifically, we adapt the VLMs with only the VPT within the visual encoder and the linear adapter on the text encoder as illustrated in Figure 1(a). Additionally, we employ an adaptive ensemble approach that determines the optimal ensemble coefficient for each domain using distances to learned classes in pre-trained VLMs (Figure 1(b)). In summary, the main contributions of this work include:

- We leverage VPT to improve class separability in visual features and TA to simultaneously enhance generalizability and adaptability, based on our comprehensive experiments examining each modality and ETL method. As far as we are aware, this is the first study to concurrently explore the behavior of VLMs across two independent lines of ETL.
- We employ an adaptive ensemble of pre- and post-adapter features to properly leverage general knowledge of VLMs for each domain, with the coefficient being adaptively determined by distances to learned classes.
- We show that **APEX** achieves state-of-the-art performance across various downstream tasks, with particularly notable improvements in unseen tasks during adaptation.

2. Related Work

Here, we provide a brief overview of the related work to our method. A detailed explanation is in Appendix E.

Transferability of Vision-Language Models. Recent VLMs [14, 23, 32, 40], which have been trained on vast image-text association pairs through self-supervised methods, have showcased impressive performance in harnessing both visual and textual information. Based on 400M and 1B of image-text pairs for pre-training of CLIP [32] and ALIGN [14], these models show higher transferability to

downstream tasks such as few-shot and zero-shot visual recognition compared to existing vision-only methods [3, 4].

Prompt Tuning. Prompt tuning is an efficient adaptation approach that automates the process of learning embeddings at the input, known as prompt tokens, rather than requiring manual prompt design. For instance, CoOp [48] fine-tunes CLIP for few-shot transfer by optimizing a continuous set of prompt vectors within its text encoder. Subsequently, several recent works [17, 39, 47] have highlighted the inferior performance of CoOp on novel classes and have sought to improve generalization. CoCoOp [47] introduces a method of conditioning prompts on image features, whereas MaPLe [16] proposes a method of learning hierarchical prompts for vision and text encoders. However, these studies do not thoroughly explore the distinct behaviors of prompt tuning across modalities, inspiring us to develop a modality-aware approach.

Adapter-style Tuning. Adapter-style tuning represents an efficient approach to adapting VLMs, which involves training an adapter network comprising one or two fully connected layers on top of the image and text encoders. CLIP-Adapter [8] proposes residual-style feature blending, integrating features from a pre-trained CLIP model with those adapted by the adapter network. Adapters that do not require training [46, 50] have recently been developed using a cache model, which is more efficient and also serves as good initialization points. However, these cache-based methods lose flexibility of VLMs as they cannot adapt to classes unseen in the training data.

3. Preliminary

Zero-shot CLIP. CLIP [32] is designed for creating visual features based on natural language guidance. The CLIP model can perform zero-shot inference, classifying an image

into one of C possible classes without additional training. This is achieved by calculating the cosine similarity between an visual feature \mathbf{z} , derived from the visual encoder, and the text features of each class $\{\mathbf{t}_i\}_{i=1}^C$, which are obtained from the text encoder.

For processing the image, let us define the visual encoder as \mathcal{V} , which comprises L_V layers, denoted as $\{\mathcal{V}_i\}_{i=1}^{L_V}$. The encoder takes patch embeddings $\mathbf{E}_0 \in \mathbb{R}^{M \times d_v}$ as input, which are obtained by dividing the image I into M fixed-size patches. Patch embeddings \mathbf{E}_i is then fed into the $(i+1)^{\text{th}}$ transformer block (\mathcal{V}_{i+1}) along with a learnable class ([CLS]) tokens \mathbf{c}_i . This process is sequentially carried out through all L_V transformer blocks, formulated as follows:

$$[\mathbf{c}_i, \mathbf{E}_i] = \mathcal{V}_i([\mathbf{c}_{i-1}, \mathbf{E}_{i-1}]) \quad i = 1, 2, \dots, L_V, \quad (1)$$

$$\mathbf{z} = \text{ImageProj}(\mathbf{c}_{L_V}), \quad (2)$$

Here, $[\cdot, \cdot]$ denotes the concatenation operation. We can obtain the text features in a similar way with word embeddings $\mathbf{W}_0 = [\mathbf{w}_0^1, \dots, \mathbf{w}_0^N] \in \mathbb{R}^{N \times d_t}$ and text encoder \mathcal{T} which is consist of L_T layers $\{\mathcal{T}_i\}_{i=1}^{L_T}$, as follows:

$$[\mathbf{W}_i] = \mathcal{T}_i(\mathbf{W}_{i-1}) \quad i = 1, 2, \dots, L_T \quad (3)$$

$$\mathbf{t}_i = \text{TextProj}(\mathbf{w}_{L_T}^N) \quad (4)$$

Then, the predicted probability for class i is formulated as

$$\Pr(y = i | \mathbf{z}, \mathbf{t}) = \frac{\exp(\text{sim}(\mathbf{z}, \mathbf{t}_i) / \tau)}{\sum_{j=1}^C \exp(\text{sim}(\mathbf{z}, \mathbf{t}_j) / \tau)}, \quad (5)$$

where $\text{sim}(\cdot, \cdot)$ indicates cosine similarity and τ is the learned temperature of CLIP. We can also interpret the text features as a **classifier** [8, 46], where \mathbf{t}_i is the classifier weight for class i .

Prompt Tuning for CLIP. To enable prompt tuning [16, 17, 47, 49], we replace the Eq. (1) and Eq. (3) by newly introducing b_V and b_T learnable tokens $\{\hat{\mathbf{P}}_i^k \in \mathbb{R}^{d_v}\}_{k=1}^{b_V}$ and $\{\mathbf{P}_i^k \in \mathbb{R}^{d_t}\}_{k=1}^{b_T}$ for i^{th} layer, and their concatenation $\hat{\mathbf{P}}_i$ and \mathbf{P}_i . We can introduce the visual prompt for the first J_V layers of the visual encoder, then we can compute as follows:

$$[\mathbf{c}_i, \mathbf{E}_i, _] = \mathcal{V}_i([\mathbf{c}_{i-1}, \mathbf{E}_{i-1}, \hat{\mathbf{P}}_{i-1}]) \quad i = 1, \dots, J_V, \quad (6)$$

$$[\mathbf{c}_j, \mathbf{E}_j, \hat{\mathbf{P}}_j] = \mathcal{V}_j([\mathbf{c}_{j-1}, \mathbf{E}_{j-1}, \hat{\mathbf{P}}_{j-1}]) \quad j = J_V + 1, \dots, L_V.$$

Similarly, we can replace Eq. (3) to belows by introducing text prompt for the first J_T layers of text encoder:

$$\begin{aligned} [_, \mathbf{W}_i] &= \mathcal{T}_i([\mathbf{P}_{i-1}, \mathbf{W}_{i-1}]) \quad i = 1, \dots, J_T, \\ [\mathbf{P}_j, \mathbf{W}_j] &= \mathcal{T}_j([\mathbf{P}_{j-1}, \mathbf{W}_{j-1}]) \quad j = J_T + 1, \dots, L_T. \end{aligned} \quad (7)$$

Here, we train the visual and text prompt for the first J_V and J_T layers of corresponding encoders.

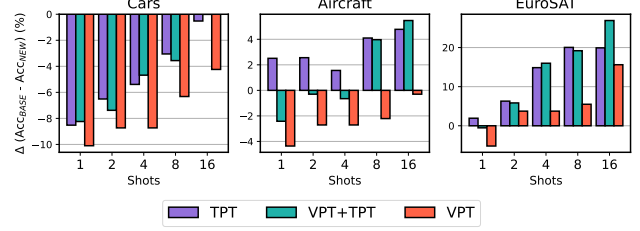


Figure 2. Comparison of accuracy differences (%) between base and novel categories across three prompt tuning options (TPT, VPT+TPT, VPT) with varying numbers of shots.

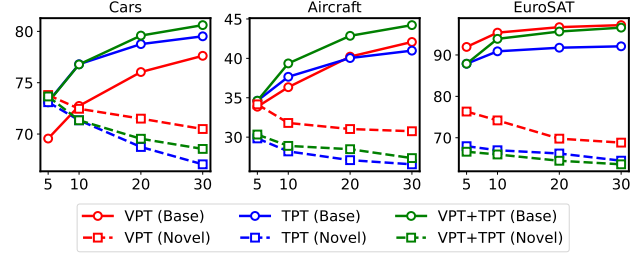


Figure 3. Comparison of the accuracy (%) of base and novel categories using TPT, VPT, and their combination (VPT+TPT) on three transfer learning datasets over various training epochs.

Adapter-style Tuning for CLIP. To enable adapter-style tuning, we replace Eq. (2) and Eq. (4) by introducing **ImageAdapter** and **TextAdapter** which are shallow stacking networks upon the frozen CLIP model [8, 46, 50].

$$\tilde{\mathbf{z}} = \text{ImageProj}(\mathbf{c}_{L_V}), \quad \mathbf{z} = \text{ImageAdapter}(\tilde{\mathbf{z}}) \quad (8)$$

$$\tilde{\mathbf{t}} = \text{TextProj}(\mathbf{w}_{L_T}^N), \quad \mathbf{t} = \text{TextAdapter}(\tilde{\mathbf{t}}) \quad (9)$$

4. Motivating Observations

In this section, we analyze the behavior of visual and text encoders within the framework of ETL to identify its optimal configuration, with more detailed values presented in Appendix D. To accomplish this, we begin by categorizing domains based on their relative transfer difficulty (RTD), which is a metric first defined by Yu et al. [42].

Definition 1 (Relative Transfer Difficulty [42]). Let $f(\cdot)$ and $g(\cdot)$ be random classifiers where the precision of each equals $1/C$, and zero-shot CLIP, respectively. Also, Prec_f and Prec_g denote the precision of classifiers f and g . Then, RTD is formulated as follows:

$$\text{RTD} = \frac{\text{Prec}_f}{\text{Prec}_g} = \frac{1/C}{\text{Prec}_g} = \frac{1}{C \cdot \text{Prec}_g}$$

Under this metric, we identify EuroSAT, DTD, and FGVC Aircraft as the three most challenging domains, while ImageNet, SUN397, and Stanford Cars are recognized as the three easiest domains. We will primarily focus on these six domains to clearly demonstrate the impact of RTD on VLMs'

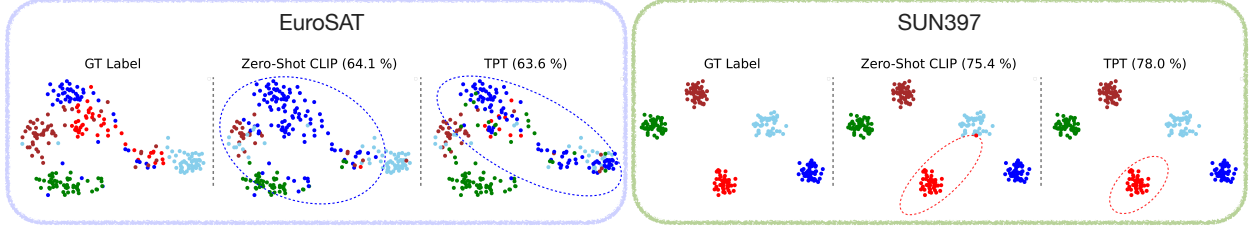


Figure 4. t-SNE [36] plots of visual features for novel category with their corresponding labels (left), zero-shot CLIP prediction (middle), and prediction with TPT (right). 50 samples are randomly selected from each class in EuroSAT and SUN397, using all 5 classes in EuroSAT and 5 randomly chosen classes from SUN397. Dotted lines within the t-SNE plot represent the decision boundaries corresponding to each class, indicated by the same color.

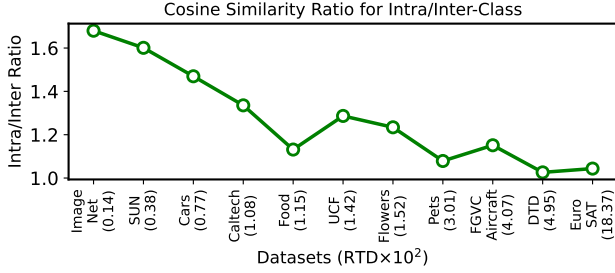


Figure 5. Comparison of intra-class and inter-class ratios to demonstrate class separability across different datasets with their RTD, arranged from low to high RTD.

behavior. To assess adaptability and generalizability, we train the CLIP-B/16 utilizing each prompt tuning approach on tasks requiring generalization from base to novel categories. Here, “base category” refers to a subset of classes within the domain learned through few-shot methods, and “novel category” is those not included in the training. Each dataset is split into these categories; the model is trained on base classes with 16 shots and tested on both.

Observation 1. *VPT offers better generalizability to unseen classes than TPT. While TPT has greater adaptability to seen classes, this adaptability comes at the risk of overfitting, which results in reduced generalizability to unseen classes.*

We commence with an analysis of the separate behavior of visual and text prompts during the tuning process. Figure 2 illustrates the performance discrepancy between the two categories for each method. Across all domains, VPT consistently shows the smallest performance gap for every shot number, indicating reduced overfitting to base classes. This observation is especially prominent in domains with high RTD though the trend is not as pronounced in domains with low RTD. We also observe that combining VPT and TPT does not consistently mitigate the overfitting of TPT, as evidenced by the larger performance gap in FGVC Aircraft and EuroSAT compared to TPT alone.

Figure 3 displays the comparative performance of base and novel categories over different epochs. While all prompt

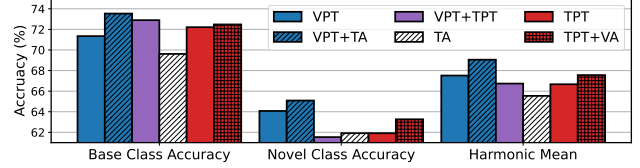


Figure 6. Comparison of the combined effectiveness of prompt tuning and adapter-style tuning.

tuning methods show an improvement in base category performance at the expense of generalization, VPT consistently exhibits a lesser decline in novel category performance. Notably, in more challenging domains like FGVC Aircraft and EuroSAT, VPT exceeds the novel performance of TPT and their combination regardless of the epoch.

Observation 2. *Low class separability of visual features is the primary reason for the overfitting of TPT on high RTD.*

Class separability is a critical factor in determining the transferability of a source model to a target domain [30]. To determine the class separability of visual features, we use the ratio of intra- to inter-class cosine similarities as a measure [29, 50]. Figure 5 demonstrates that the ratio is higher in domains with lower RTD, which are considered easier, and lower in more challenging datasets with higher RTD. These findings suggest that the class separability highly correlates with transfer difficulty, strongly influencing the overfitting risk of TPT on high RTD domains.

To see how class separability affects TPT, we further explore the visual features and predictions of zero-shot CLIP and TPT. As illustrated in Figure 4, EuroSAT, which exhibits a high RTD, shows lower class separability compared to SUN397 that has a lower RTD. Furthermore, in EuroSAT, when TPT attempts to classify visual features with low class separability, its performance for novel classes is lower than zero-shot CLIP. This is because TPT tries to fit the decision boundary, represented as dotted lines, to features that are challenging to classify by solely adjusting classifier weights with multiple stacks of learnable prompts. Consequently, this leads to significant overfitting, where the decision boundary of one class overlaps with others. Conversely, with visual

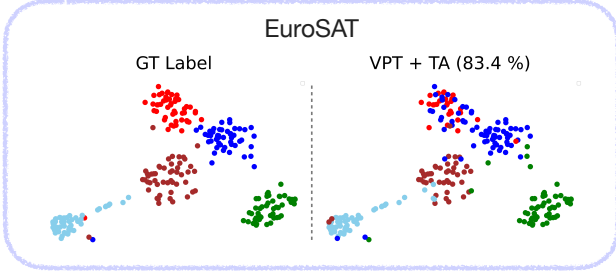


Figure 7. t-SNE plots of visual features of CLIP with VPT for a novel category with their corresponding labels (left) and prediction with TA (right). 50 samples are randomly selected from each class.

features that exhibit high class separability, TPT’s predictions are more accurate than those of zero-shot CLIP as it can easily determine the better decision boundary. These results underscore the significance of separable visual features, a factor closely linked to VPT.

Observation 3. *TA effectively enhances adaptability with low risk of overfitting when employed with VPT.*

Figure 6 shows that while TA and VPT each exhibit less adaptability than TPT alone, together they outperform across all categories, signifying both high adaptability and a low overfitting risk. This synergy occurs because VPT enhances the class separability in visual features, allowing the linear transformation of classifier weights to suffice for adaptation, as depicted in Figure 7. TA simply modifies the features of the pretrained text encoder, preventing overconfidence in the decision boundary especially for domains with high RTD and low class separability. In addition, we conduct experiments using a combination of TPT and a visual adapter (VA). However, this combination proves less effective than integrating VPT and TA, further emphasizing the importance of visual feature separability.

Observation 4. *By modulating TA through an ensemble of pre-adapter and post-adapter features, each with a domain-specific coefficient, we can significantly improve generalization in low RTD domains while maintaining high performance in high RTD domains.*

While combining VPT and TA can mitigate overfitting, utilizing TA can still result in the loss of some general knowledge from the original CLIP. This is evident in Table 1, as naively using VPT and TA together may lead to a degradation in performance on novel classes in domains with low RTD. This is because for low RTD, a lot of tasks within the domain need to lie in the region of general knowledge, as illustrated in Figure 1(b). But the training of a TA creates a task-specific boundary which may not be optimal for other tasks within the same domain. In domains with high RTD, task-specific knowledge gained from adapters can also enhance performance on unseen tasks, as the general knowledge is often insufficient for these domains.

Table 1. Comparison of accuracy (%) on novel classes between zero-shot CLIP, without an ensemble, an ensemble with fixed coefficient, and an ensemble with optimal coefficient. We determine the fixed coefficient as 0.4, based on average novel performance.

Dataset	SUN397	Stanford Cars	DTD	EuroSAT
ZS CLIP	75.35	74.89	59.90	64.05
VPT + TA	74.52 (-0.83)	68.40 (-6.49)	63.05 (+3.15)	77.73 (+13.68)
+ Fixed Ens ($\alpha = 0.4$)	78.68 (+3.33)	74.22 (-0.67)	64.16 (+4.26)	75.87 (+11.82)
+ Opt. Ens	78.90 (+3.55)	75.19 (+0.30)	64.32 (+4.42)	77.73 (+13.68)
Opt. α	0.3	0.0	0.5	1.0

This degradation in domains with low RTD can be mitigated by diminishing the influence of TA. Inspired by the residual connection in adapter-style tuning methods [8, 46], we utilize an ensemble of pre-adapter and post-adapter features for the text encoder. This ensemble, defined with the coefficient α , can be expressed as:

$$\mathbf{t} = \alpha \cdot \mathbf{TextAdapter}(\tilde{\mathbf{t}}) + (1 - \alpha) \cdot \tilde{\mathbf{t}}. \quad (10)$$

As Table 1 illustrates, the ensemble method improves performance in domains with low RTD. However, using a fixed coefficient α , set at 0.4 for optimal average performance, can lead to suboptimal results in some domains. For example, it causes a performance drop from 77.73% to 75.87% on EuroSAT, as high RTD domains require more from TA. By setting α optimally for each domain, we consistently surpass zero-shot CLIP across all domains, effectively combining general and task-specific knowledge tailored to each domain. These findings highlight the necessity of a method to calculate an adaptive coefficient of ensemble, which would modulate TA activation according to domain and its RTD.

5. Method

5.1. Configuration Design & Training

Due to the need for VPT for class separability and TA for adaptability, we configure the trainable parameters to include multiple stacks of visual prompts, and a linear text adaptation layer following the pretrained text encoder. While existing adapter-style methods [8, 46, 50] rely on manually optimized text prompts for different datasets, we use learnable text prompts just for the input because manually creating prompt templates for each domain in the real world is challenging. The learnable text prompts are unnecessary if manual prompts are already well-formed, which is further explained in Section 6.

We extract the visual feature \mathbf{z} using Eq. (6) and Eq. (2) and the text feature \mathbf{t} using Eq. (7) with $J_T = 1$ and Eq. (9). We apply linear adapter parameterized as matrix \mathbf{A} and bias

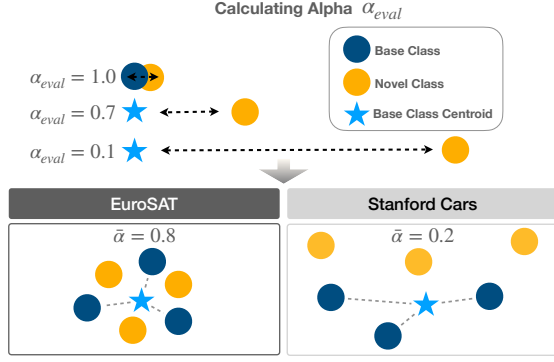


Figure 8. An overview of our method for calculating the adaptive coefficient α_{eval} for ensemble, based on class distance.

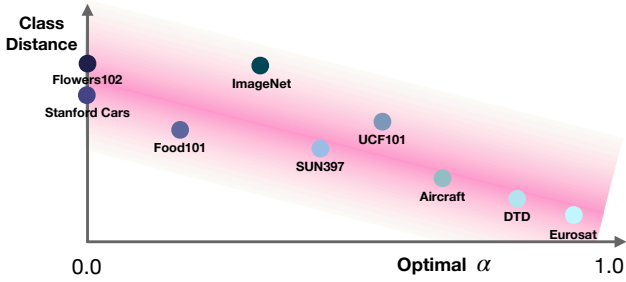


Figure 9. The relationship between class distance and optimal α for each domain used in Eq. (10) and Table 1. Oxford Pets and Caltech101 are excluded from here since their performance does not depend on α .

\mathbf{b} for **TextAdapter** in Eq. (9) rather than using bottleneck structure [8, 46] based on our results in Figure 10. Our adapter can be formulated as follows:

$$\mathbf{t} = \text{TextAdapter}(\tilde{\mathbf{t}}) := \mathbf{A}^T \tilde{\mathbf{t}} + \mathbf{b} \quad (11)$$

During the training procedure, our objective is to maximize the predicted probability $\Pr(y = y_{\text{gt}} | \mathbf{z}, \mathbf{t})$ for ground truth label y_{gt} by using cross-entropy loss $\ell_{\text{CE}}(\mathbf{z}, \mathbf{t}, y_{\text{gt}})$ which is defined as follows:

$$\ell_{\text{CE}}(\mathbf{z}, \mathbf{t}, y_{\text{gt}}) = \log \Pr(y = y_{\text{gt}} | \mathbf{z}, \mathbf{t}),$$

where the predicted probability is computed as Eq. (5).

5.2. Adaptive Ensemble for Evaluation

Motivated by Obs. 4, in the evaluation stage, we use an adaptive ensemble approach that combines pre-adapter ($\tilde{\mathbf{t}}_{\text{eval}}$) and post-adapter text features (Eq. (11)), described as follows:

$$\mathbf{t}_{\text{eval}} = \alpha_{\text{eval}} \cdot (\mathbf{A}^T \tilde{\mathbf{t}}_{\text{eval}} + \mathbf{b}) + (1 - \alpha_{\text{eval}}) \cdot \tilde{\mathbf{t}}_{\text{eval}},$$

where α_{eval} is the ensemble coefficient for a target class at evaluation and \mathbf{t}_{eval} is the final representation for that class.

To determine the optimal α_{eval} for each class, we employ a non-parametric method based on the distance between the

text features of the evaluation class and the classes learned during training. This approach is grounded in the assumption that target features considered as out-of-task features should rely more on general knowledge of pretrained VLMs, while features closer to the learned classes should utilize more task-specific knowledge. With regard to this, we adaptively set α_{eval} by comparing the text feature of the evaluation class with the features of the learned classes, as illustrated in Figure 8. Specifically, we calculate both the average and nearest distances between the evaluation class and the C learned classes in the following manner:

$$d_{\text{eval}}^{\text{avg}} = 1.0 - \frac{1}{C} \sum_{j=1}^C \text{sim}(\mathbf{t}'_{\text{eval}}, \mathbf{t}'_j),$$

$$d_{\text{eval}}^{\text{nn}} = 1.0 - \min_{j \in \{1, \dots, C\}} \text{sim}(\mathbf{t}'_{\text{eval}}, \mathbf{t}'_j),$$

where $\mathbf{t}'_{\text{eval}}$ and \mathbf{t}'_j indicate text feature of evaluation class and learned class $j \in \{1, \dots, C\}$ from pretrained VLMs and sim denotes cosine similarity. Using these distance metrics, we compute the coefficient α_{eval} as follows:

$$\alpha_{\text{eval}} = \exp \left(-\beta \cdot (d_{\text{eval}}^{\text{avg}}) \cdot \mathbf{1}_{(d_{\text{eval}}^{\text{nn}} > \epsilon)} \right),$$

where β is a scaling factor. The equation indicates a preference for pre-adapter features when the text feature distance from learned classes is large, and for trained TA when it is small. The condition of $d_{\text{eval}}^{\text{nn}} > \epsilon$, where ϵ is a small value set at 0.05, serves to treat an evaluation class that is very similar to the base class as identical. This adaptive α_{eval} enables flexible use of general and task-specific knowledge.

Although α_{eval} is calculated class-wisely, it also relates to the target domain and its corresponding RTD. In domains with high RTD, class features are typically less separable in the text embedding space. Consequently, domains like EuroSAT exhibit low class distances, while those with low RTD, like Stanford Cars, display high class distances. Figure 9 demonstrates that the optimal α , used in Eq. (10) and Table 1, is strongly correlated with the distance between class features. This relationship between class distance and the optimal α suggests that α_{eval} can effectively represent transfer difficulty.

Additionally, to further improve the performance, we also employ an ensemble technique for the visual encoder that combines the visual feature of the pretrained VLM (\mathbf{z}') with the task-adapted VLMs (\mathbf{z}) as follows:

$$\mathbf{z} = \bar{\alpha} \cdot \mathbf{z}' + (1 - \bar{\alpha}) \cdot \mathbf{z},$$

$\bar{\alpha}$, the mean value of α_{eval} , is used for image ensemble since class-specific α_{eval} cannot be applied at the image level.

There are two main differences between our ensemble approach and the residual connection of CLIP-Adapter [8] or

Tip-Adapter [46]. *Firstly*, instead of training with these ensembled features, we apply them only during the evaluation stage which can be more effective for unseen classes during the training while preserving the performance of learned classes. *Secondly*, in previous works, the ensemble coefficient is either manually tuned for each dataset [46] or treated as a learnable parameter [8]. However, these approaches are impractical because the dataset encountered during the evaluation stage is unknown. Instead, we adjust the adaptive coefficient based on the distance between the features of evaluation classes and the features of learned classes.

6. Experiments

6.1. Experimental Setup

Datasets. We evaluate **APEX** on the three most commonly used transfer learning tasks: base-to-novel generalization, cross-dataset evaluation, and domain generalization. For all the few-shot experiments except domain generalization, we follow CoCoOp [47] which uses 11 image recognition datasets. The datasets cover multiple recognition tasks including ImageNet [6] and Caltech101 [7] which consists of generic objects; OxfordPets [31], Stanford Cars [18], Flowers102 [28], Food101 [2], and FGVC Aircraft [27] for fine-grained classification, SUN397 [38] for scene recognition, UCF101 [34] for action recognition, DTD [5] for texture classification, and EuroSAT [11] which consists of satellite images. For the domain generalization benchmark, we use ImageNet as a source dataset and use ImageNet-A [12], ImageNet-R [13], ImageNet-Sketch [37], and ImageNetV2 [33] as out-of-domain datasets.

Experimental Details. We use multiple baselines for comparison with our methods in experiments. These include the standard zero-shot CLIP [32], CLIP-Adapter [8], CoCoOp [47] and MaPLE [16]. We also consider ProGrad [49], which uses gradient alignment for prompt learning. When reporting results, we have reproduced all the experiments, as we observe that the values are highly dependent on the random seed. Instead of taking the average results from three seeds, as done in previous works [16], we use the **average of 20 seeds** to determine the final value for base-to-novel and the **average of 5 seeds** for cross-evaluation and domain-generalization. Additionally, we found that using the Adadelta optimizer [44] yields better results, so we have reproduced the experiments with Adadelta. More experimental details can be found in the Appendix A.

6.2. Main Results

Base-to-Novel Generalization. In this scenario, the datasets are evenly divided into base and novel categories. The model is trained on the base classes using 16 shots and is subsequently tested on both the base and novel classes. As indicated in Table 2, **APEX** consistently outperforms the best of

Table 2. Accuracy comparison on base-to-novel generalization of **APEX** with previous methods.

Dataset		CLIP	CLIP-Adapter	CoCoOp	MaPLE	ProGrad	APEX
Average on 11 datasets	Base	69.34	83.23	81.11	82.52	82.55	83.99
	Novel	74.22	70.13	70.55	74.24	72.20	76.76
	HM	71.70	75.64	75.03	77.86	76.77	80.04
ImageNet	Base	72.43	76.06	76.47	77.02	76.97	77.12
	Novel	68.14	68.40	69.60	70.15	67.20	71.10
	HM	70.22	72.03	72.87	73.42	71.75	73.99
Caltech101	Base	96.84	98.00	97.70	97.95	97.88	98.18
	Novel	94.00	93.66	93.96	94.60	93.57	95.06
	HM	95.40	95.78	95.78	96.25	95.68	96.59
OxfordPets	Base	91.17	94.86	95.66	95.80	95.00	95.11
	Novel	97.26	94.49	96.32	97.82	97.46	97.27
	HM	94.12	94.67	95.99	96.80	96.21	96.18
Stanford Cars	Base	63.37	77.62	72.92	74.69	78.64	80.53
	Novel	74.89	68.53	71.98	73.53	70.23	75.08
	HM	68.65	72.79	72.45	74.11	74.20	77.71
Flowers102	Base	72.08	96.88	94.82	95.90	94.83	97.47
	Novel	77.80	69.20	70.71	72.96	74.70	77.58
	HM	74.83	80.73	81.01	82.87	83.57	86.40
Food101	Base	90.10	90.02	90.63	90.46	90.40	89.60
	Novel	91.22	89.76	91.13	91.71	90.43	92.06
	HM	74.83	89.89	90.88	91.08	90.41	90.81
FGVC Aircraft	Base	27.19	40.14	36.19	37.76	40.77	42.69
	Novel	36.29	31.77	26.82	34.67	30.16	35.21
	HM	31.09	35.47	30.81	36.15	34.67	38.59
SUN397	Base	69.36	81.72	80.55	81.33	81.19	81.17
	Novel	75.35	73.54	75.48	77.75	73.42	78.98
	HM	72.23	77.41	77.93	79.50	77.11	80.06
DTD	Base	53.24	81.77	77.34	79.34	76.64	82.45
	Novel	59.90	49.02	48.86	56.64	54.23	63.80
	HM	56.37	61.29	59.89	66.10	63.52	71.94
EuroSAT	Base	56.48	91.55	87.05	93.00	91.23	92.83
	Novel	64.05	61.10	61.27	69.17	68.58	79.89
	HM	60.03	73.29	71.92	79.33	78.30	85.88
UCF101	Base	70.53	86.87	82.86	84.43	84.54	86.74
	Novel	77.50	71.94	69.92	77.64	74.24	78.37
	HM	73.85	78.70	75.84	80.89	79.06	82.34

the previous methods in average accuracy across all datasets, with a margin of 1~6%. In particular, our method exhibits superior performance in novel classes on all datasets, demonstrating **APEX**'s enhanced generalizability. The exceptions are Oxford Pets and FGVC Aircraft, where the performance is already exceptionally high and low, respectively. This improvement is especially notable in domains with high RTD, such as EuroSAT (+15.84%) and DTD (+3.90%). Additionally, the **APEX** method also shows superior performance in base categories, highlighting the high adaptability of our proposed approach.

Table 3. Comparison of accuracy on cross-dataset of **APEX** with previous methods.

Dataset		C-Adapter	CoCoOp	MaPLE	ProGrad	APEX
Source	ImageNet	70.12	71.46	70.58	71.73	72.00
Target	Caltech101	92.94	93.24	93.46	93.30	94.46
	OxfordPets	86.80	90.38	90.28	89.95	90.06
	Cars	64.22	64.08	65.22	65.25	65.46
	Flower102	69.06	70.50	71.80	69.34	71.58
	Food101	85.20	85.64	86.24	86.22	86.44
	Aircraft	24.24	21.58	23.62	21.22	24.44
	SUN397	64.36	66.30	67.32	65.32	67.20
	DTD	43.44	43.68	45.04	42.19	45.70
	EuroSAT	47.66	45.48	46.24	45.33	47.58
	UCF101	65.52	67.42	68.26	67.62	68.80
Average		64.34	64.83	65.75	64.57	66.16

Table 4. Comparison of accuracy on domain generalization of **APEX** with previous methods.

	Source	Target				
	ImageNet	-V2	-S	-A	-R	Avg.
C-Adapter	70.12	61.78	46.70	48.56	74.00	57.76
CoCoOp	71.46	64.44	48.58	50.20	75.64	59.72
MaPLE	70.58	63.95	48.78	50.53	76.78	59.90
ProGrad	71.73	64.54	48.59	50.38	75.87	59.85
APEX	72.00	64.70	48.48	50.68	76.76	60.16

Cross-dataset Evaluation. We train the model to generalize across different domains by using a cross-dataset evaluation task. Specifically, we first train the model on the ImageNet dataset and then transfer it to the 10 other datasets. Table 3 summarizes that **APEX** shows the best overall performance compared to existing baselines. Our proposed method achieves the best performance on 7 out of 11 tasks. This demonstrates **APEX**'s effectiveness, especially in difficult situations where both the task and domain are unseen.

Domain Generalization. We assess the capability of our method to generalize to out-of-distribution data by training on the source dataset, ImageNet, and subsequently testing on various modified versions of ImageNet. Our method does not achieve a large margin of superiority since our adaptive ensemble is primarily designed to enhance performance in novel classes. Nonetheless, our method still surpasses all baseline models on average accuracy in this domain generalization task.

6.3. Ablation Study

In this section, we provide ablation experiments on **APEX**. Full results on each dataset is detailed in Appendix C.

Effect of Ensemble. We have conducted a component analysis of two adaptive ensemble techniques of **APEX**, focusing on (1) the text encoder and (2) the visual encoder. The results, as shown in Table 5, reveal that the ensembling of

Table 5. Comparison of the effect of adaptive ensemble technique between text and visual encoder by RTD.

Text	Visual	Easy	Challenge	All
✗	✗	70.67	58.25	74.61
✓	✗	74.51 (+3.84)	58.66 (+0.41)	76.19 (+1.58)
✗	✓	70.79 (+0.12)	58.65 (+0.40)	74.83 (+0.22)
✓	✓	75.05 (+4.38)	59.63 (+1.38)	76.76 (+2.15)

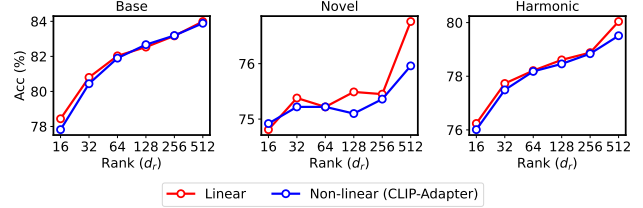


Figure 10. Comparison of the accuracy of base, novel, and their harmonic mean using low-rank linear adapter and bottleneck layer of non-linear adapter [8].

the text encoder is crucial for enhancing performance. Conversely, ensembling the visual encoder results in a minor yet consistent improvement. The text ensemble notably achieves substantial improvements in domains with low RTD, implying that task-specific knowledge is primarily acquired through TA. Overall, employing both ensemble techniques leads to the most improvement regardless of RTD.

Using Low-Rank Linear Adapter. CLIP-Adapter [8] and Tip-Adapter [46] utilize the bottleneck layer [10] which shrinks and re-expands the feature dimensions to improve efficiency. Similarly, we utilize low-rank matrix factorization that $\mathbf{A} = \mathbf{U}\mathbf{V}^\top$ where $\mathbf{V}, \mathbf{U} \in \mathbb{R}^{d_l \times d_r}$ with $d_r < d_l$ to improve the parameter efficiency. Figure 10 shows that although TA's performance diminishes with decreasing dimension d_r , average accuracy with few parameters ($d_r = 32$) still achieves performance comparable to ProGrad [49] (+0.72%). We also observe that the linear adapter consistently outperforms the non-linear adapter [8] across all values of d_r , motivating us to use a linear adapter in our proposed **APEX**.

Shallow Prompt. Although we observe that TPT leads to overfitting, we employ one-layer learnable text prompts to enhance real-world practicality. Table 6 compares the performance of manually optimized prompts [8, 46], the ensemble of manual prompts [32], and shallow prompts. The shallow prompt method outperforms manual prompts, proving its effectiveness. However, manual prompts, particularly when ensembled, also show comparable performance to shallow prompts, suggesting that well-designed manual prompts can be an effective alternative.

Table 6. Comparison of the accuracy of the base, novel, and their harmonic means among the various prompt types on text encoder.

Prompt	Base Acc.	Novel Acc.	HM
Opt. manual prompt [46]	84.15	75.24	79.17
Ens. (60 manual prompts [32])	84.02	76.17	79.70
Shallow prompt	83.99	76.76	80.04

7. Conclusion

We propose **APEX** to address the challenges of conventional prompt and adapter-style tuning methods for ETL for VLMs. Our approach incorporates two key components based on our observations: (1) using VPT and TA for exploiting the property of each modality and (2) adaptive ensemble coefficient in the inference stage. We empirically demonstrate the superior performance of **APEX**, consistently achieving a better performance than the previous methods.

References

- [1] Jean-Baptiste Alayrac, Jeff Donahue, Pauline Luc, Antoine Miech, Iain Barr, Yana Hasson, Karel Lenc, Arthur Mensch, Katherine Millican, Malcolm Reynolds, et al. Flamingo: a visual language model for few-shot learning. *Advances in Neural Information Processing Systems*, 35:23716–23736, 2022. 8
- [2] Lukas Bossard, Matthieu Guillaumin, and Luc Van Gool. Food-101 - mining discriminative components with random forests. In *European Conference on Computer Vision*, 2014. 7
- [3] Ting Chen, Simon Kornblith, Mohammad Norouzi, and Geoffrey Hinton. A simple framework for contrastive learning of visual representations. In *International conference on machine learning*, pages 1597–1607. PMLR, 2020. 2
- [4] Xinlei Chen, Saining Xie, and Kaiming He. An empirical study of training self-supervised vision transformers. In *Proceedings of the IEEE/CVF International Conference on Computer Vision (ICCV)*, pages 9640–9649, 2021. 2
- [5] Mircea Cimpoi, Subhransu Maji, Iasonas Kokkinos, Sammy Mohamed, and Andrea Vedaldi. Describing textures in the wild. *2014 IEEE Conference on Computer Vision and Pattern Recognition*, pages 3606–3613, 2013. 7
- [6] Jia Deng, Wei Dong, Richard Socher, Li-Jia Li, Kai Li, and Fei-Fei Li. Imagenet: a large-scale hierarchical image database. pages 248–255, 2009. 7
- [7] Li Fei-Fei, Rob Fergus, and Pietro Perona. Learning generative visual models from few training examples: An incremental bayesian approach tested on 101 object categories. *2004 Conference on Computer Vision and Pattern Recognition Workshop*, pages 178–178, 2004. 7
- [8] Peng Gao, Shijie Geng, Renrui Zhang, Teli Ma, Rongyao Fang, Yongfeng Zhang, Hongsheng Li, and Yu Qiao. Clip-adapter: Better vision-language models with feature adapters. *International Journal of Computer Vision*, pages 1–15, 2023. 1, 2, 3, 5, 6, 7, 8, 4
- [9] Shashank Goel, Hritik Bansal, Sumit Bhatia, Ryan Rossi, Vishwa Vinay, and Aditya Grover. Cyclip: Cyclic contrastive language-image pretraining. *Advances in Neural Information Processing Systems*, 35:6704–6719, 2022. 7
- [10] Kaiming He, Xiangyu Zhang, Shaoqing Ren, and Jian Sun. Deep residual learning for image recognition. In *Proceedings of the IEEE conference on computer vision and pattern recognition*, pages 770–778, 2016. 8
- [11] Patrick Helber, Benjamin Bischke, Andreas R. Dengel, and Damian Borth. Eurosat: A novel dataset and deep learning benchmark for land use and land cover classification. *IEEE Journal of Selected Topics in Applied Earth Observations and Remote Sensing*, 12:2217–2226, 2017. 7
- [12] Dan Hendrycks, Kevin Zhao, Steven Basart, Jacob Steinhardt, and Dawn Xiaodong Song. Natural adversarial examples. *2021 IEEE/CVF Conference on Computer Vision and Pattern Recognition (CVPR)*, pages 15257–15266, 2019. 7
- [13] Dan Hendrycks, Steven Basart, Norman Mu, Saurav Kada-vath, Frank Wang, Evan Dorundo, Rahul Desai, Tyler Lixuan Zhu, Samyak Parajuli, Mike Guo, Dawn Xiaodong Song, Jacob Steinhardt, and Justin Gilmer. The many faces of robustness: A critical analysis of out-of-distribution generalization. *2021 IEEE/CVF International Conference on Computer Vision (ICCV)*, pages 8320–8329, 2020. 7
- [14] Chao Jia, Yinfei Yang, Ye Xia, Yi-Ting Chen, Zarana Parekh, Hieu Pham, Quoc Le, Yun-Hsuan Sung, Zhen Li, and Tom Duerig. Scaling up visual and vision-language representation learning with noisy text supervision. In *International conference on machine learning*, pages 4904–4916. PMLR, 2021. 1, 2, 6
- [15] Menglin Jia, Luming Tang, Bor-Chun Chen, Claire Cardie, Serge Belongie, Bharath Hariharan, and Ser-Nam Lim. Visual prompt tuning. In *European Conference on Computer Vision (ECCV)*, 2022. 8
- [16] Muhammad Uzair khattak, Hanoona Rasheed, Muhammad Maaz, Salman Khan, and Fahad Shahbaz Khan. Maple: Multi-modal prompt learning. In *The IEEE/CVF Conference on Computer Vision and Pattern Recognition*, 2023. 1, 2, 3, 7, 8
- [17] Muhammad Uzair Khattak, Syed Talal Wasim, Muzammal Naseer, Salman Khan, Ming-Hsuan Yang, and Fahad Shahbaz Khan. Self-regulating prompts: Foundational model adaptation without forgetting. In *Proceedings of the IEEE/CVF International Conference on Computer Vision*, pages 15190–15200, 2023. 1, 2, 3, 5, 8
- [18] Jonathan Krause, Michael Stark, Jia Deng, and Li Fei-Fei. 3d object representations for fine-grained categorization. *2013 IEEE International Conference on Computer Vision Workshops*, pages 554–561, 2013. 7
- [19] Brian Lester, Rami Al-Rfou, and Noah Constant. The power of scale for parameter-efficient prompt tuning. In *Proceedings of the 2021 Conference on Empirical Methods in Natural Language Processing*, pages 3045–3059, Online and Punta Cana, Dominican Republic, 2021. Association for Computational Linguistics. 8
- [20] Junnan Li, Ramprasaath Selvaraju, Akhilesh Gotmare, Shafiq Joty, Caiming Xiong, and Steven Chu Hong Hoi. Align before fuse: Vision and language representation learning with

- momentum distillation. *Advances in neural information processing systems*, 34:9694–9705, 2021. 8
- [21] Junnan Li, Dongxu Li, Caiming Xiong, and Steven Hoi. Blip: Bootstrapping language-image pre-training for unified vision-language understanding and generation. In *International Conference on Machine Learning*, pages 12888–12900. PMLR, 2022. 7
- [22] Liunian Harold Li, Pengchuan Zhang, Haotian Zhang, Jianwei Yang, Chunyuan Li, Yiwu Zhong, Lijuan Wang, Lu Yuan, Lei Zhang, Jenq-Neng Hwang, et al. Grounded language-image pre-training. In *Proceedings of the IEEE/CVF Conference on Computer Vision and Pattern Recognition*, pages 10965–10975, 2022. 7
- [23] Yangguang Li, Feng Liang, Lichen Zhao, Yufeng Cui, Wanli Ouyang, Jing Shao, Fengwei Yu, and Junjie Yan. Supervision exists everywhere: A data efficient contrastive language-image pre-training paradigm. In *International Conference on Learning Representations*, 2022. 2
- [24] Yanghao Li, Haoqi Fan, Ronghang Hu, Christoph Feichtenhofer, and Kaiming He. Scaling language-image pre-training via masking. In *Proceedings of the IEEE/CVF Conference on Computer Vision and Pattern Recognition*, pages 23390–23400, 2023. 7
- [25] Xuejing Liu, Wei Tang, Jinghui Lu, Rui Zhao, Zhaojun Guo, and Fei Tan. Deeply coupled cross-modal prompt learning. *arXiv preprint arXiv:2305.17903*, 2023. 8
- [26] Yuning Lu, Jianzhuang Liu, Yonggang Zhang, Yajing Liu, and Xinmei Tian. Prompt distribution learning. In *Proceedings of the IEEE/CVF Conference on Computer Vision and Pattern Recognition*, pages 5206–5215, 2022. 8
- [27] Subhransu Maji, Esa Rahtu, Juho Kannala, Matthew B. Blaschko, and Andrea Vedaldi. Fine-grained visual classification of aircraft. *ArXiv*, abs/1306.5151, 2013. 7
- [28] Maria-Elena Nilsback and Andrew Zisserman. Automated flower classification over a large number of classes. *2008 Sixth Indian Conference on Computer Vision, Graphics & Image Processing*, pages 722–729, 2008. 7
- [29] Jaehoon Oh, Hyungjun Yoo, ChangHwan Kim, and Se-Young Yun. {BOIL}: Towards representation change for few-shot learning. In *International Conference on Learning Representations*, 2021. 4
- [30] Michal Pándy, Andrea Agostinelli, Jasper Uijlings, Vittorio Ferrari, and Thomas Mensink. Transferability estimation using bhattacharyya class separability. In *Proceedings of the IEEE/CVF Conference on Computer Vision and Pattern Recognition*, pages 9172–9182, 2022. 4
- [31] Omkar M. Parkhi, Andrea Vedaldi, Andrew Zisserman, and C. V. Jawahar. Cats and dogs. *2012 IEEE Conference on Computer Vision and Pattern Recognition*, pages 3498–3505, 2012. 7
- [32] Alec Radford, Jong Wook Kim, Chris Hallacy, Aditya Ramesh, Gabriel Goh, Sandhini Agarwal, Girish Sastry, Amanda Askell, Pamela Mishkin, Jack Clark, et al. Learning transferable visual models from natural language supervision. In *International conference on machine learning*, pages 8748–8763. PMLR, 2021. 1, 2, 7, 8, 9, 3, 4, 6
- [33] Benjamin Recht, Rebecca Roelofs, Ludwig Schmidt, and Vaishaal Shankar. Do imagenet classifiers generalize to imagenet? In *International Conference on Machine Learning*, 2019. 7
- [34] Khurram Soomro, Amir Roshan Zamir, and Mubarak Shah. Ucf101: A dataset of 101 human actions classes from videos in the wild. *ArXiv*, abs/1212.0402, 2012. 7
- [35] Quan Sun, Yuxin Fang, Ledell Wu, Xinlong Wang, and Yue Cao. Eva-clip: Improved training techniques for clip at scale. *arXiv preprint arXiv:2303.15389*, 2023. 6, 7
- [36] Laurens Van der Maaten and Geoffrey Hinton. Visualizing data using t-sne. *Journal of machine learning research*, 9(11), 2008. 4
- [37] Haohan Wang, Songwei Ge, Eric P. Xing, and Zachary Chase Lipton. Learning robust global representations by penalizing local predictive power. In *Neural Information Processing Systems*, 2019. 7
- [38] Jianxiong Xiao, James Hays, Krista A. Ehinger, Aude Oliva, and Antonio Torralba. Sun database: Large-scale scene recognition from abbey to zoo. *2010 IEEE Computer Society Conference on Computer Vision and Pattern Recognition*, pages 3485–3492, 2010. 7
- [39] Hantao Yao, Rui Zhang, and Changsheng Xu. Visual-language prompt tuning with knowledge-guided context optimization. In *Proceedings of the IEEE/CVF Conference on Computer Vision and Pattern Recognition*, pages 6757–6767, 2023. 2, 8
- [40] Lewei Yao, Runhui Huang, Lu Hou, Guansong Lu, Minzhe Niu, Hang Xu, Xiaodan Liang, Zhenguo Li, Xin Jiang, and Chunjing Xu. FILIP: Fine-grained interactive language-image pre-training. In *International Conference on Learning Representations*, 2022. 2, 7
- [41] Jiahui Yu, Zirui Wang, Vijay Vasudevan, Legg Yeung, Mojtaba Seyedhosseini, and Yonghui Wu. Coca: Contrastive captioners are image-text foundation models. *arXiv preprint arXiv:2205.01917*, 2022. 6, 7
- [42] Tao Yu, Zhihe Lu, Xin Jin, Zhibo Chen, and Xinchao Wang. Task residual for tuning vision-language models. In *Proceedings of the IEEE/CVF Conference on Computer Vision and Pattern Recognition*, pages 10899–10909, 2023. 3, 8
- [43] Yuhang Zang, Wei Li, Kaiyang Zhou, Chen Huang, and Chen Change Loy. Unified vision and language prompt learning. *arXiv preprint arXiv:2210.07225*, 2022. 8
- [44] Matthew D Zeiler. Adadelta: an adaptive learning rate method. *arXiv preprint arXiv:1212.5701*, 2012. 7, 1
- [45] Xiaohua Zhai, Basil Mustafa, Alexander Kolesnikov, and Lucas Beyer. Sigmoid loss for language image pre-training. *arXiv preprint arXiv:2303.15343*, 2023. 7
- [46] Renrui Zhang, Wei Zhang, Rongyao Fang, Peng Gao, Kunchang Li, Jifeng Dai, Yu Qiao, and Hongsheng Li. Tip-adapter: Training-free adaption of clip for few-shot classification. In *Computer Vision – ECCV 2022*, pages 493–510, Cham, 2022. Springer Nature Switzerland. 1, 2, 3, 5, 6, 7, 8, 9, 4
- [47] Kaiyang Zhou, Jingkang Yang, Chen Change Loy, and Ziwei Liu. Conditional prompt learning for vision-language models. In *Proceedings of the IEEE/CVF Conference on Computer*

Vision and Pattern Recognition, pages 16816–16825, 2022. 1, 2, 3, 7, 8

- [48] Kaiyang Zhou, Jingkang Yang, Chen Change Loy, and Ziwei Liu. Learning to prompt for vision-language models. *International Journal of Computer Vision*, 130(9):2337–2348, 2022. 1, 2, 8

- [49] Beier Zhu, Yulei Niu, Yucheng Han, Yue Wu, and Hanwang Zhang. Prompt-aligned gradient for prompt tuning. In *Proceedings of the IEEE/CVF International Conference on Computer Vision*, pages 15659–15669, 2023. 3, 7, 8

- [50] Xiangyang Zhu, Renrui Zhang, Bowei He, Aojun Zhou, Dong Wang, Bin Zhao, and Peng Gao. Not all features matter: Enhancing few-shot clip with adaptive prior refinement. In *Proceedings of the IEEE/CVF International Conference on Computer Vision (ICCV)*, pages 2605–2615, 2023. 1, 2, 3, 4, 5, 8

Improving Adaptability and Generalizability of Efficient Transfer Learning for Vision-Language Models

Supplementary Material

A. Implementation Details

As explained in Section 6, we utilize the ViT-B/16 model as the CLIP image encoder and a standard GPT2-like structure with an End Of Text (EOT) token as the classification token for the text encoder. To implement **APEX**, we use visual prompts for all layers, setting $J_V = 12$ for base-to-novel generalization and $J_V = 3$ for cross-evaluation and domain generalization. The text prompt is applied only to the shallow prompt, and therefore, $J_T = 1$ for all experiments. The number of prompts for each layer, b_V and b_T , is set to 2. The initial text prompt is fixed as “a photo of a”, and the visual prompts are initialized with a zero-mean Gaussian distribution with a standard deviation of 0.02. The matrix term of the text adapter is initialized with an identity matrix, and the bias vector is initialized with a zero vector.

For training, we use the Adadelta optimizer [44] with a learning rate of 0.15 and a cosine learning rate scheduler. The batch size is set to 16, and we train for 15 epochs, except for ImageNet, where we train for 5 epochs. As in previous works, we apply augmentation techniques of random cropping and flipping. The scaling factor β , used for calculating α_{eval} , is set to 4.0. In the SGD experiments presented in Appendix C, we adopt a batch size of 16 and epochs of 30 and 5 for ImageNet, along with a learning rate of 0.0015 and a cosine learning rate scheduler. The augmentation and scaling factors are set the same as in the Adadelta experiments.

For reproducing baselines, we use the Adadelta optimizer with a learning rate of 0.25, selected after a grid search with values [0.1, 0.15, 0.2, 0.25, 0.3]. The rest of the settings remain the same as in the original papers. Results with their original configurations using SGD optimizer are listed in Appendix C. All our experiments were conducted on a single NVIDIA RTX 3090.

B. Notation and Algorithm

In this section, we present the notation and algorithm of our method, **APEX**. The notation is detailed in Table 7. The training algorithm for **APEX** is outlined in Algorithm 1, and the adaptive inference algorithm is presented in Algorithm 2.

Table 7. The notation table for Section 4

Notation	Description
<i>The notation for VLMs</i>	
\mathcal{V}	The visual encoder of VLMs
\mathcal{T}	The text encoder of VLMs
L_V	The number of layers of visual encoder
L_T	The number of layers of text encoder
\mathcal{V}_ℓ	The ℓ^{th} Transformer layer of visual encoder
\mathcal{T}_ℓ	The ℓ^{th} Transformer layer of text encoder
\mathbf{E}_ℓ	The patch embeddings of ℓ^{th} layer of visual encoder
\mathbf{W}_ℓ	The word embeddings of ℓ^{th} layer of text encoder
<i>The inputs for VLMs or prompt tuning</i>	
J_V	The number of layers of VPT
J_T	The number of layers of TPT
b_V	The context length of VPT
b_T	The context length of TPT
$\hat{\mathbf{P}}_\ell$	The visual prompt of ℓ^{th} layer of visual encoder
\mathbf{P}_ℓ	The text prompt of ℓ^{th} layer of text encoder
<i>The outputs for VLMs</i>	
\mathbf{c}_ℓ	The embedded features of ℓ^{th} layer for [CLS] token
\mathbf{t}_i	The text features of i^{th} class
\mathbf{z}	The visual features from visual encoder
<i>The outputs for VLMs related to APEX</i>	
\mathbf{z}'	The visual features from visual encoder of pretrained VLMs for adaptive ensemble
\mathbf{t}'	The text features from text encoder of pretrained VLMs for adaptive ensemble
$\tilde{\mathbf{t}}$	The pre-adapter text features of text encoder of adapted VLMs

Algorithm 1 Pseudo-Algorithm for Training of **APEX**

Require: Pretrained visual encoder \mathcal{V} , Pretrained text encoder \mathcal{T} , Learnable vision prompts $\hat{\mathbf{P}}$, Shallow text prompts \mathbf{P}_0 , Adapter parameterized by matrix \mathbf{A} and \mathbf{b}

Require: Training Samples \mathcal{S} , Initial Text Embeddings \mathbf{W}_0

- 1: Randomly initialize $\phi = [\hat{\mathbf{P}}, \mathbf{A}, \mathbf{b}]$
- 2: **while** not done **do**
- 3: Sample Batch $\mathcal{B} = (I, y_{gt})$
- 4: $\mathbf{E}_0 = \text{PathEmbedding}(I)$
- 5: **for** $i = 1, \dots, J_V$ **do**
- 6: $[\mathbf{c}_i, \mathbf{E}_i, _] \leftarrow \mathcal{V}_i([\mathbf{c}_{i-1}, \mathbf{E}_{i-1}, \hat{\mathbf{P}}_{i-1}])$
- 7: **end for**
- 8: **for** $i = J_V + 1, \dots, L_V$ **do**
- 9: $[\mathbf{c}_i, \mathbf{E}_i, \hat{\mathbf{P}}_i] \leftarrow \mathcal{V}_i([\mathbf{c}_{i-1}, \mathbf{E}_{i-1}, \hat{\mathbf{P}}_{i-1}])$
- 10: **end for**
- 11: $\mathbf{z} \leftarrow \text{ImageProj}(\mathbf{c}_{L_V})$
- 12: $\tilde{\mathbf{t}} = \mathcal{T}([\mathbf{W}_0, \mathbf{P}_0])$
- 13: $\mathbf{t} = \mathbf{A}^\top \tilde{\mathbf{t}} + \mathbf{b}$
- 14: /* Calculate the probability for class i */
- 15: $\Pr(y = i | \mathbf{z}, \mathbf{t}) = \frac{\exp(\text{sim}(\mathbf{z}, \mathbf{t}_i) / \tau)}{\sum_{j=1}^C \exp(\text{sim}(\mathbf{z}, \mathbf{t}_j) / \tau)}$
- 16: $\ell_{\text{CE}}(\mathbf{z}, \mathbf{t}, y_{gt}) = \log \Pr(y = y_{gt} | \mathbf{z}, \mathbf{t})$
- 17: $\phi = \phi - \gamma \nabla_{\phi} \ell_{\text{CE}}(\mathbf{z}, \mathbf{t}, y_{gt}; \phi)$
- 18: **end while**

C. Additional Experiments**C.1. Full Results of Ablation on Ensemble**

Table 8. Full results for novel classes on each dataset of Table 5.

Visual Text	\times \times	\times \checkmark	\checkmark \times	$\checkmark(\text{APEX})$ $\checkmark(\text{APEX})$
ImageNet	69.08	70.09	69.22	71.10
Caltech101	94.91	94.80	95.01	95.06
OxfordPets	97.24	97.39	97.07	97.27
Cars	68.40	74.46	68.32	75.08
Flower102	73.71	76.40	74.43	77.58
Food101	90.70	91.83	90.82	92.06
Aircraft	33.97	33.89	33.87	35.21
SUN397	74.52	78.98	74.82	78.98
DTD	63.05	63.05	63.82	63.80
EuroSAT	77.73	79.04	78.25	79.89
UCF101	77.39	78.17	77.55	78.37
Average	74.61	76.19	74.83	76.76

Table 8 illustrates the complete results of the component analysis of the adaptive ensemble, which are summarized in Table 5. We only display results for novel classes, as these ensemble components do not affect the results for base classes, given that α_{eval} is set to 1.0 for seen classes. As previously explained, the ensemble of the text encoder is crucial as its removal leads to a significant performance drop in domains

Algorithm 2 Pseudo-Algorithm for Adaptive Inference of **APEX**

Require: Pretrained visual encoder \mathcal{V} , Pretrained text encoder \mathcal{T} , Learned vision prompts $\hat{\mathbf{P}}$, Learned shallow text prompts \mathbf{P}_0 , Learned adapter parameterized by matrix \mathbf{A} and \mathbf{b} , The C classes for base category $\{1, \dots, C\}$, The C_{eval} candidate classes for evaluation $\{C + 1, \dots, C + C_{eval}\}$,

Require: Initial Trained Text Embeddings $\{\mathbf{W}_{0,j}\}_{j=1}^C$, Initial Evaluation Text Embedding $\{\mathbf{W}_{0,eval}\}_{eval=C+1}^{C+C_{eval}}$, Evaluation Image I

- 1: $\{\mathbf{t}'_j\}_{j=1}^C = \{\mathcal{T}(\mathbf{W}_{0,j})\}_{j=1}^C$
- 2: **for** $eval = C + 1, \dots, C + C_{eval}$ **do**
- 3: $\mathbf{t}'_{eval} = \mathcal{T}(\mathbf{W}_{0,eval})$
- 4: $\tilde{\mathbf{t}}_{eval} = \mathcal{T}([\mathbf{W}_{0,eval}, \mathbf{P}_0])$
- 5: $d_{eval}^{avg} = 1.0 - \frac{1}{C} \sum_{j=1}^C \text{sim}(\mathbf{t}'_{eval}, \mathbf{t}'_j)$
- 6: $d_{eval}^{mn} = 1.0 - \min_{j \in \{1, \dots, C\}} \text{sim}(\mathbf{t}'_{eval}, \mathbf{t}'_j)$
- 7: $\alpha_{eval} = \exp(-\beta \cdot (d_{eval}^{avg} \cdot \mathbf{1}_{(d_{eval}^{mn} > \epsilon)})$
- 8: $\mathbf{t}_{eval} = \alpha_{eval} \cdot (\mathbf{A}^\top \tilde{\mathbf{t}}_{eval} + \mathbf{b}) + (1 - \alpha_{eval}) \cdot \tilde{\mathbf{t}}_{eval}$
- 9: **end for**
- 10: $\mathbf{E}_0 = \text{PathEmbedding}(I)$
- 11: $\mathbf{c}'_{L_V} = \mathcal{V}([\mathbf{c}_0, \mathbf{E}_0])$
- 12: $\mathbf{z}' \leftarrow \text{ImageProj}(\mathbf{c}'_{L_V})$
- 13: **for** $i = 1, \dots, J_V$ **do**
- 14: $[\mathbf{c}_i, \mathbf{E}_i, _] \leftarrow \mathcal{V}_i([\mathbf{c}_{i-1}, \mathbf{E}_{i-1}, \hat{\mathbf{P}}_{i-1}])$
- 15: **end for**
- 16: **for** $i = J_V + 1, \dots, L_V$ **do**
- 17: $[\mathbf{c}_i, \mathbf{E}_i, \hat{\mathbf{P}}_i] \leftarrow \mathcal{V}_i([\mathbf{c}_{i-1}, \mathbf{E}_{i-1}, \hat{\mathbf{P}}_{i-1}])$
- 18: **end for**
- 19: $\mathbf{z} \leftarrow \text{ImageProj}(\mathbf{c}_{L_V})$
- 20: $\bar{\alpha} = \frac{1}{C_{eval}} \sum_{eval=C+1}^{C+C_{eval}} \alpha_{eval}$
- 21: $\mathbf{z} = \bar{\alpha} \cdot \mathbf{z}' + (1 - \bar{\alpha}) \cdot \mathbf{z}$
- 22: /* Calculate the probability for class i */
- 23: Calculate $\Pr(y = i | \mathbf{z}, \mathbf{t}) = \frac{\exp(\text{sim}(\mathbf{z}, \mathbf{t}_i) / \tau)}{\sum_{j=C+1}^{C+C_{eval}} \exp(\text{sim}(\mathbf{z}, \mathbf{t}_j) / \tau)}$
- 24: Predict as $\arg \max_{i \in \{C+1, \dots, C+C_{eval}\}} \Pr(y = i | \mathbf{z}, \mathbf{t})$

with low RTD, such as Stanford Cars and SUN397. This demonstrates that moderating TA with an adaptive ensemble helps to leverage both task-specific knowledge and general VLMs knowledge effectively. The ensemble on the visual encoder offers marginal improvement, but combining both still yields the most superior performance on average.

C.2. Full Results on Low-Rank Experiments

Figure 11 presents detailed results for each dataset using low-rank methods, which are summarized in Figure 10. Consistent with the findings shown in Figure 10, Figure 11 demonstrates that our linear adapter provides better overall results, particularly for novel classes across most datasets. This parameter-efficient approach exhibits relative robust-

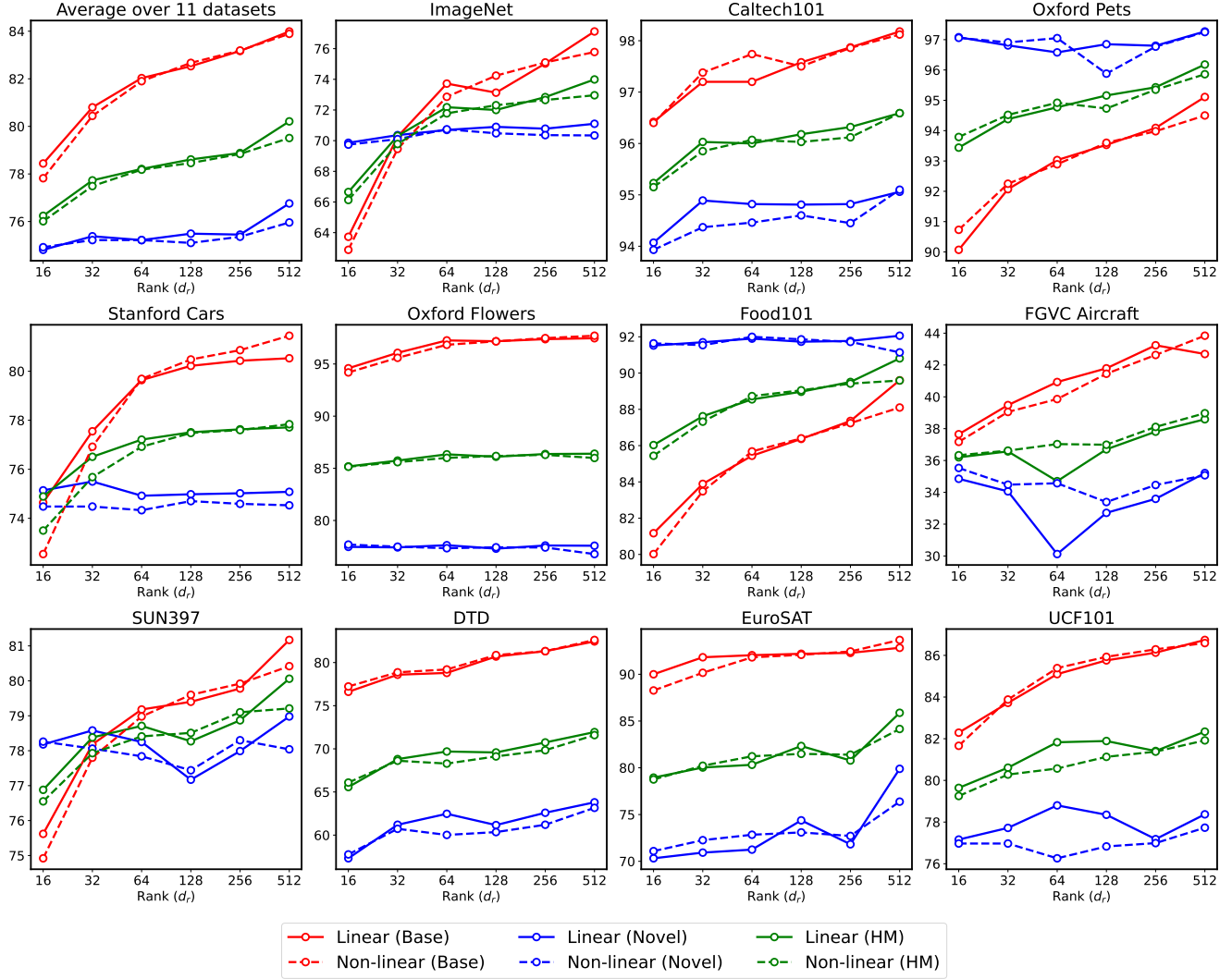


Figure 11. Extended results for individual datasets of Figure 10.

Table 9. Full results on each dataset of Table 6

		Average on 11 datasets	ImageNet	Caltech101	OxfordPets	Stanford Cars	Flowers102	Food101	FGVC Aircraft	SUN397	DTD	EuroSAT	UCF101
Opt. manual prompt [46]	Base	84.15	76.64	98.15	95.05	80.75	97.45	89.35	42.92	81.24	83.02	93.93	87.10
	Novel	75.24	69.00	94.33	97.04	75.32	77.66	91.28	36.42	77.60	57.59	71.74	79.70
	HM	79.17	72.62	96.20	96.03	77.94	86.44	90.30	39.40	79.38	68.01	81.35	83.24
Ens. (60 manual prompts) [32]	Base	84.02	76.48	98.15	95.09	80.70	97.37	89.56	42.56	81.46	82.62	93.01	87.18
	Novel	76.17	70.24	93.93	96.44	75.88	77.16	91.20	35.64	78.36	59.45	80.35	79.21
	HM	79.70	73.23	95.99	95.76	78.22	86.09	90.37	38.79	79.88	69.15	86.22	83.00
Shallow prompt (APEX)	Base	83.99	77.12	98.18	95.11	80.53	97.47	89.60	42.69	81.17	82.45	92.83	86.74
	Novel	76.76	71.10	95.06	97.27	75.08	77.58	92.06	35.21	78.98	63.80	79.89	78.37
	HM	80.04	73.99	96.59	96.18	77.71	86.40	90.81	38.59	80.06	71.94	85.88	82.34

ness in performance, even outperforming MaPLe [16] for rank 64 (+0.32%) on average. These encouraging results have led us to adopt the linear adapter for the text encoder. Furthermore, we observe that initializing the adapter with an

identity matrix improves performance, a strategy that can be explored more thoroughly in future work.

Table 10. Comparison of baselines using their own configuration (SGD optimizer) with our method.

Dataset		CLIP	CLIP -Adapter	Co -CoOp	MaPLE	Pro -Grad	APEX
Average on 11 datasets	Base	69.34	81.81	80.28	81.74	81.78	84.04
	Novel	74.22	71.43	72.03	73.89	69.42	75.67
	HM	71.70	75.93	75.60	77.30	74.80	79.42
ImageNet	Base	72.43	74.40	75.99	76.81	76.93	76.93
	Novel	68.14	68.63	70.39	70.66	69.51	69.61
	HM	70.22	71.40	73.08	73.61	73.03	73.09
Caltech101	Base	96.84	97.61	97.64	95.61	95.41	98.18
	Novel	94.00	93.72	94.52	94.71	94.05	95.02
	HM	95.40	95.63	96.05	96.18	95.90	96.57
OxfordPets	Base	91.17	95.06	95.56	95.61	95.41	95.21
	Novel	97.26	95.02	97.52	97.63	90.56	97.74
	HM	94.12	95.04	96.53	96.61	92.92	96.46
Stanford Cars	Base	63.37	76.18	70.97	72.49	77.41	80.44
	Novel	74.89	69.30	73.44	73.46	70.92	74.76
	HM	68.65	72.58	72.18	72.97	74.02	77.50
Flowers102	Base	72.08	96.27	93.88	95.49	95.34	97.73
	Novel	77.80	69.92	72.56	72.55	76.84	76.67
	HM	74.83	81.01	81.85	82.45	85.10	85.93
Food101	Base	90.10	90.32	90.54	90.50	90.17	89.46
	Novel	91.22	90.10	91.15	91.71	85.53	91.94
	HM	74.83	90.21	90.84	91.10	87.79	90.68
FGVC Aircraft	Base	27.19	38.87	33.64	36.33	39.01	42.96
	Novel	36.29	31.95	26.49	32.64	27.77	34.72
	HM	31.09	35.07	29.64	34.39	32.44	38.40
SUN397	Base	69.36	76.50	79.86	80.65	81.35	81.18
	Novel	75.35	74.60	76.51	78.33	69.06	77.08
	HM	72.23	75.54	78.15	79.47	74.70	79.08
DTD	Base	53.24	80.46	76.58	79.20	77.45	82.19
	Novel	59.90	52.79	53.47	55.01	51.63	61.21
	HM	56.37	63.75	62.97	64.92	61.96	70.17
EuroSAT	Base	56.48	88.48	86.18	90.38	84.88	93.48
	Novel	64.05	67.12	63.04	68.43	56.66	75.88
	HM	60.03	76.33	72.82	77.89	67.96	83.77
UCF101	Base	70.53	85.81	82.22	84.02	83.82	86.71
	Novel	77.50	72.55	73.22	77.62	71.13	77.77
	HM	73.85	78.62	77.46	80.69	76.96	82.00

C.3. Full Results on Manual Text Prompts

Table 9 presents the detailed results for each dataset using manual prompts, which are summarized in Table 6. The manual prompts, designed for each dataset as described in [8, 46], appear to underperform compared to other methods. This suggests that they may not be the optimal choice for every dataset, and that designing these prompts manually is challenging. In contrast, just ensembling multiple manual prompts [32] works significantly better, indicating that optimal prompts may exist among these manual options. This finding also implies that utilizing improved manual prompts can substantially enhance performance, potentially replacing

Table 11. Extended baselines not presented in Table 2 for comparison between base-to-novel experiments with our method.

Dataset		CLIP	VPT	TPT	VPT + TPT	Prompt -SRC	APEX
Average on 11 datasets	Base	69.34	81.01	82.07	82.93	84.36	83.99
	Novel	74.22	73.11	73.90	74.15	75.37	76.76
	HM	71.70	76.55	77.51	78.00	79.39	80.04
ImageNet	Base	72.43	75.94	76.81	77.18	77.90	77.12
	Novel	68.14	68.74	69.45	69.86	70.26	71.10
	HM	70.22	72.16	72.94	73.34	73.88	73.99
Caltech101	Base	96.84	97.79	97.84	97.98	97.81	98.18
	Novel	94.00	93.65	94.29	94.38	93.88	95.06
	HM	95.40	95.68	96.03	96.15	95.80	96.59
OxfordPets	Base	91.17	95.11	95.48	95.78	95.69	95.11
	Novel	97.26	96.57	97.52	97.65	97.42	97.27
	HM	94.12	95.83	96.49	96.71	96.55	96.18
Stanford Cars	Base	63.37	70.72	75.18	75.75	80.16	80.53
	Novel	74.89	72.78	72.73	73.02	74.52	75.08
	HM	68.65	71.74	73.93	74.36	77.24	77.71
Flowers102	Base	72.08	91.60	96.45	96.26	96.96	97.47
	Novel	77.80	69.62	74.69	72.62	76.73	77.58
	HM	74.83	79.11	84.19	82.79	85.67	86.40
Food101	Base	90.10	90.17	90.30	90.36	90.60	89.60
	Novel	91.22	90.94	91.42	91.58	91.38	92.06
	HM	90.66	90.55	90.86	90.97	90.99	90.81
FGVC Aircraft	Base	27.19	34.70	37.86	38.76	43.67	42.69
	Novel	36.29	33.53	34.17	35.08	36.42	35.21
	HM	31.09	34.10	35.92	36.83	39.72	38.59
SUN397	Base	69.36	79.09	81.70	81.57	82.94	81.17
	Novel	75.35	76.85	77.62	77.92	78.37	78.98
	HM	72.23	77.95	79.61	79.70	80.59	80.06
DTD	Base	53.24	78.67	79.81	80.81	82.21	82.45
	Novel	59.90	53.78	55.32	55.64	59.58	63.80
	HM	56.37	63.89	65.35	65.90	69.09	71.94
EuroSAT	Base	56.48	94.17	86.98	92.91	93.06	92.83
	Novel	64.05	73.26	69.16	71.19	71.60	79.89
	HM	60.03	82.41	77.05	80.61	80.93	85.88
UCF101	Base	70.53	83.10	84.38	84.92	87.05	86.74
	Novel	77.50	74.52	76.54	76.75	78.96	78.37
	HM	73.85	78.58	80.27	80.63	82.81	82.34

shallow prompts. Shallow prompt tuning for the text input yields the best results, demonstrating its effectiveness and flexibility. Therefore, we adopt this approach for our main results.

C.4. Baseline Results with SGD

Table 10 displays the reproduced results using the SGD optimizer, in contrast to the Adadelta optimizer presented in Table 2. As observed, the results with SGD are slightly lower

Table 12. Results for additional ablation study on configurations when combined with adaptive ensemble.

		Average on 11 datasets	ImageNet	Caltech101	OxfordPets	Stanford Cars	Flowers102	Food101	FGVC Aircraft	SUN397	DTD	EuroSAT	UCF101
TPT + VA	Base	83.51	76.43	98.00	94.76	79.68	97.28	89.24	42.27	80.96	81.49	92.27	86.24
	Novel	75.88	69.43	94.49	97.21	75.77	77.50	91.50	34.85	78.20	62.05	76.77	76.90
	HM	79.32	72.76	96.21	95.97	77.68	86.27	90.36	38.20	79.56	70.45	83.81	81.30
VPT + TA + TPT	Base	83.56	76.93	98.03	94.77	79.45	97.51	89.26	42.14	81.02	81.72	92.11	86.21
	Novel	75.09	71.30	94.72	97.76	72.98	76.70	91.94	33.80	78.08	58.82	73.11	76.80
	HM	78.85	74.01	96.35	96.24	76.08	85.86	90.58	37.51	79.52	68.40	81.52	81.23
VPT + TA (APEX)	Base	83.99	77.12	98.18	95.11	80.53	97.47	89.60	42.69	81.17	82.45	92.83	86.74
	Novel	76.76	71.10	95.06	97.27	75.08	77.58	92.06	35.21	78.98	63.80	79.89	78.37
	HM	80.04	73.99	96.59	96.18	77.71	86.40	90.81	38.59	80.06	71.94	85.88	82.34

Table 13. Results for additional ablation study on scaling factor β . Our proposed methods shows robust performance on the selection of β .

β	Average on 11 datasets	ImageNet	Caltech101	OxfordPets	Stanford Cars	Flowers102	Food101	FGVC Aircraft	SUN397	DTD	EuroSAT	UCF101
1.0	75.97	70.62	95.15	97.43	72.15	75.95	91.38	35.07	77.02	63.90	78.36	78.66
2.0	76.51	71.06	95.14	97.44	73.95	77.06	91.70	35.35	78.12	63.99	78.89	78.92
3.0	76.75	71.18	95.15	97.37	74.69	77.61	91.92	35.46	78.66	64.17	79.35	78.64
4.0 (APEX)	76.76	71.10	95.06	97.27	75.08	77.58	92.06	35.21	78.98	63.80	79.89	78.37
5.0	76.72	71.00	95.16	97.18	75.10	77.79	91.96	35.05	78.96	63.77	79.88	78.07
6.0	76.66	70.96	95.16	97.15	75.17	77.80	91.98	34.84	78.92	63.54	80.01	77.75

compared to those with Adadelta. This difference is likely due to the adaptive learning rate of Adadelta, which facilitates training in this unstable few-shot scenario. Nonetheless, even with the SGD optimizer, our method significantly outperforms all baselines, particularly in domains with high RTD, maintaining the same trend observed with the Adadelta optimizer.

C.5. Comparison with More Baselines

Due to the page limit, we present a comparison with additional baselines for base-to-novel generalization experiments in Table 11, which are not included in Table 2. These include training with VPT, TPT, and a combination of VPT and TPT. We also compare our method with the recently proposed PromptSRC [17], which employs various regularization techniques such as self-consistency loss and Gaussian averaging. Our method outperforms all these baselines in terms of harmonic mean and demonstrates particularly high performance for novel classes. Compared to PromptSRC, our method significantly outperforms in novel classes of high RTD domains, such as EuroSAT (+8.39%) and DTD (+4.22%), while maintaining comparable performance in other domains. Notably, our method achieves these results with a simpler training approach, without the need for numerous manual prompts for SRC loss, and with fewer hyperparameters, unlike the many required by PromptSRC’s regularization techniques. Additionally, our method surpasses the simpler baselines of naive training using VPT, TPT, and their combination, highlighting the effectiveness of our configuration design

and adaptive ensemble.

C.6. Ablation on Configuration

To further analyze the optimal configuration in combination with an adaptive ensemble, we conduct additional ablation studies on configurations. The results, present in Table 12, show that utilizing VPT and TA yields the best outcomes, confirming their effectiveness when paired with the adaptive ensemble. However, adding TPT to VPT and TA does not enhance performance, especially in high RTD scenarios, as evidenced by decreased performance in DTD (-4.98%) and EuroSAT (-6.78%) compared to configurations without TPT. While combining TPT with VA demonstrates reasonable performance, it is not as effective as the combination of VPT and TA. This highlights the importance of class separability of visual features achieved through multiple stacks of prompts. Overall, the configuration of **APEX** outperforms the other setups.

C.7. Ablation on β

Table 13 presents the results of an ablation study on the hyperparameter β , which is used to calculate α_{eval} . A higher β leads to a lower α_{eval} , indicating greater reliance on the general knowledge of VLMs, which is beneficial for domains with low RTD, and vice versa. As observed, the performance in domains with low RTD, such as Stanford Cars and SUN397, tends to improve with a higher β . However, the optimal performance for difficult domains like Aircraft and DTD is achieved with β values between 1.0 and 3.0.

Table 14. Extended results for ablation study on hyperparamter α related to Table 1.

α	Average on 11 datasets	ImageNet	Caltech101	OxfordPets	Stanford Cars	Flowers102	Food101	FGVC Aircraft	SUN397	DTD	EuroSAT	UCF101
0.0	75.38	70.80	95.13	97.03	75.19	77.87	91.94	33.57	78.32	61.68	70.90	76.80
0.1	75.86	71.06	95.19	97.19	75.17	77.67	92.10	34.34	78.82	62.68	72.74	77.52
0.2	76.10	71.20	95.14	97.29	75.04	77.52	91.96	34.75	78.80	63.18	74.10	78.08
0.3	76.27	71.20	95.09	97.39	74.67	77.33	91.92	35.16	78.90	63.74	75.08	78.54
0.4	76.34	71.18	95.14	97.47	74.22	76.96	91.88	35.34	78.68	64.16	75.87	78.84
0.5	76.29	71.04	95.15	97.50	73.59	76.56	91.78	35.45	78.40	64.32	76.41	79.01
0.6	76.13	70.82	95.14	97.47	72.74	76.13	91.64	35.33	78.00	64.30	76.95	78.96
0.7	75.88	70.46	95.17	97.39	71.82	75.66	91.44	35.25	77.38	64.23	77.10	78.79
0.8	75.54	70.06	95.07	97.36	70.85	75.09	91.22	34.93	76.56	64.04	77.33	78.39
0.9	75.10	69.62	95.01	97.31	69.63	74.49	90.98	34.53	75.68	63.53	77.44	77.92
1.0	74.61	69.08	94.91	97.24	68.40	73.71	90.70	33.97	74.52	63.05	77.73	77.39

Not all domains follow this tendency since α_{eval} is calculated on a class-wise basis, as demonstrated in the case of EuroSAT. Interestingly, except for the value of 2.0, our method demonstrates robustness to variations in β , as it does not significantly affect the average performance. Overall, setting β to 4.0 yields the best performance, and therefore, this value has been selected for the final results.

C.8. Ablation on α

Table 14 presents the comprehensive results of the ablation study on a fixed α , which is used in Table 1 and Eq. (10). The same α is applied uniformly across all classes and is set as a fixed value for both the visual and text encoders. This is done to determine the correlation between α and the domain, along with its transfer difficulty. Similar to Section C.7, domains with high RTD, such as EuroSAT, require a higher α value to perform well compared to domains with low RTD, like Stanford Cars. These findings support the necessity for an adaptive ensemble that is closely aligned with RTD.

C.9. Results on Different VLMs

We validate our approach using different backbones: EVA-CLIP [35] and CoCa [41]. Table 15 displays the results using these two backbones, where we compare our method with both zero-shot and naive prompt tuning approaches that combine VPT and TPT. As observed, **APEX** consistently outperforms the average results in terms of harmonic mean, regardless of the model used. Specifically, with EVA-CLIP, our method demonstrates superior performance for both base and novel classes. In the case of the most challenging domain, EuroSAT, our method significantly enhances performance compared to the zero-shot accuracy for novel classes (+18.46%). A similar improvement of 8.85% on EuroSAT is observed with CoCa. However, in terms of novel classes, the average performance of zero-shot tuning is superior for CoCa. This could be attributed to the larger patch size of this backbone, which might increase the risk of overfitting on the

vision side when setting two learnable prompts. Nonetheless, our method shows comparable performance on novel classes to zero-shot CoCa, with a significant improvement in base classes. This results in superior performance in harmonic mean, demonstrating our method’s effectiveness across various VLMs.

D. Details about Observation

D.1. Relative Transfer Difficulty

Here, we report the value of RTD which is defined in Section 4 for 11 transfer datasets. We compute the RTD based on the CLIP-B/16 model.

D.2. Inter- and Intra-class Cosine Similarity

In addition to presenting relative values in Figure 5, we also report the absolute values for both inter- and intra-class similarities. We observe a significant correlation between the RTD and the ratio of intra- to inter-class similarity.

D.3. Results on 6 datasets

We also present extended results in Figure 12, which include data from three additional datasets: ImageNet, SUN397, and DTD. For ImageNet and SUN397, which already exhibit high class separability, we note that all methods—TPT, VPT, and their combination—yield similar performance differences. However, the results for DTD indicate a tendency for TPT to overfit to the base classes. This observation is consistent with the findings presented in Figure 2.

E. More Related Work

Vision-Language Models VLMs overcome the limitations of vision-only supervised learning with their robustness and flexibility in zero-shot inference through natural language supervision. CLIP [32] facilitates this by adopting contrastive learning with a large-scale dataset of 400 million images. ALIGN[14] further improves upon this by scaling up the

Table 15. Accuracy on base-to-novel generalization of **APEX** on EVA-CLIP [35] and CoCa [41].

Model		EVA-CLIP-B/16			CoCa-B/32		
Dataset		ZS	TPT +VPT	APEX	ZS	TPT +VPT	APEX
Average on 11 datasets	Base	75.28	85.91	85.93	70.85	82.39	82.09
	Novel	77.68	75.24	79.34	74.29	71.05	73.98
	HM	76.46	80.22	82.50	72.53	76.30	77.87
ImageNet	Base	79.20	81.78	81.26	67.10	69.50	69.46
	Novel	75.60	72.28	75.83	66.60	62.33	66.46
	HM	77.36	76.74	78.45	66.85	65.72	67.90
Caltech101	Base	98.60	98.87	98.82	96.70	97.86	98.04
	Novel	97.30	95.05	97.22	96.30	94.12	95.98
	HM	97.95	96.92	98.01	96.50	95.95	97.00
OxfordPets	Base	94.90	95.52	95.27	92.30	91.83	92.44
	Novel	98.10	98.34	97.97	96.20	95.07	93.54
	HM	96.47	96.91	96.60	94.21	93.42	92.99
Stanford Cars	Base	76.90	85.76	86.16	84.00	88.94	88.87
	Novel	87.10	82.49	86.75	93.00	90.73	92.57
	HM	81.68	84.09	86.45	88.27	89.83	90.68
Flowers102	Base	74.20	99.41	99.50	69.10	96.33	96.83
	Novel	81.10	77.32	79.94	74.70	65.61	70.09
	HM	77.50	86.98	88.65	71.79	78.06	81.32
Food101	Base	90.30	90.34	90.24	81.20	79.87	80.80
	Novel	91.90	90.11	91.76	82.90	79.30	82.66
	HM	91.09	90.22	90.99	82.04	79.58	81.72
FGVC Aircraft	Base	28.70	45.52	46.01	21.40	40.71	39.81
	Novel	32.50	26.75	32.12	25.50	22.04	25.22
	HM	30.48	33.70	37.83	23.27	28.60	30.88
SUN397	Base	76.70	83.10	82.44	73.70	78.68	77.68
	Novel	80.80	76.76	80.54	77.40	73.50	77.12
	HM	78.70	79.80	81.48	75.50	76.00	77.40
DTD	Base	62.80	83.78	84.15	62.60	83.04	83.25
	Novel	63.90	61.32	64.39	61.10	58.46	61.14
	HM	63.35	70.81	72.96	61.84	68.62	70.50
EuroSAT	Base	72.30	95.32	94.81	62.80	96.42	93.87
	Novel	68.30	73.74	86.76	71.50	73.90	80.35
	HM	70.24	83.15	90.61	66.87	83.67	86.59
UCF101	Base	73.50	85.58	86.58	68.50	83.13	82.01
	Novel	77.90	73.43	79.49	72.00	66.54	69.69
	HM	75.64	79.04	82.88	70.21	73.92	74.76

dataset with more noisy image-text pairs. FILIP [40] enables finer-grained alignment between two modalities and GLIP [22] improves visual grounding and object detection using VLMs. CoCa [41] employs both captioning and contrastive losses, thereby integrating the model capabilities of contrastive approaches like CLIP with those of generative methods. CyCLIP [9] employs cyclic loss to ensure geomet-

Table 16. The relative transfer difficulty values for all datasets by using Definition 1.

Dataset	ImageNet	Caltech	Pets	Cars
RTD	1.4×10^{-3}	1.08×10^{-2}	3.01×10^{-2}	7.7×10^{-3}
Dataset	Flowers	Food	Aircraft	SUN
RTD	1.52×10^{-2}	1.15×10^{-2}	4.07×10^{-2}	3.8×10^{-3}
Dataset	DTD	EuroSAT	UCF	
RTD	4.95×10^{-3}	1.84×10^{-1}	1.42×10^{-2}	

Table 17. The averaged cosine similarity value for inter- and intra-class and their relative ratio.

Dataset	ImageNet	Caltech	Pets	Cars	Flowers	Food
Inter	0.551	0.672	0.844	0.564	0.749	0.754
Intra	0.925	0.898	0.910	0.829	0.924	0.853
Ratio	1.680	1.336	1.078	1.470	1.234	1.131
Dataset	Aircraft	SUN	DTD	EuroSAT	UCF	
Inter	0.746	0.487	0.803	0.896	0.673	
Intra	0.858	0.780	0.823	0.934	0.866	
Ratio	1.150	1.602	1.025	1.042	1.287	

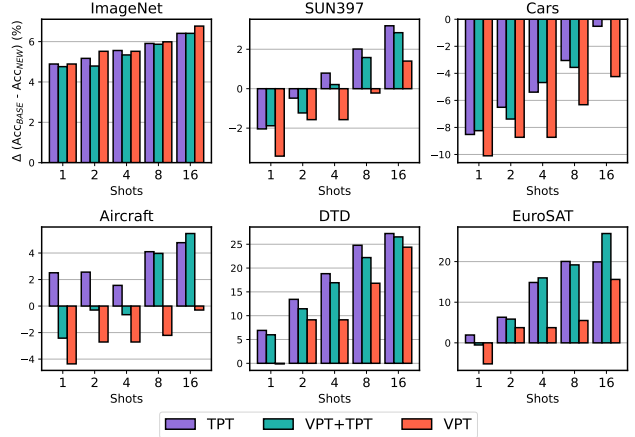


Figure 12. Extended results for Figure 2. All results in different datasets show similar trends that indicate **VPT** yields a smaller discrepancy in performance between base and novel categories, suggesting a reduced risk of overfitting compared to **TPT**.

ric consistency, while FLIP [24] enhances VLMs through masking techniques. EVA-CLIP [35] implements various training techniques, such as different attention mechanisms and optimizers, to further improve CLIP’s performance. Additionally, SigLIP [45] replaces the softmax loss with sigmoid loss, enabling more efficient pretraining with smaller batch sizes.

There is also a line of research focused on encoder-decoder or decoder-only architectures. BLIP [21] facilitates both encoding and decoding by training with three objective functions, utilizing synthetic data and data fil-

tering. ALBEF [20] employs a strategy of alignment before applying cross-attention, combined with a momentum update. Flamingo [1] enables few-shot inference in vision-language tasks through architectural innovations, using vision-language prompts.

Prompt Tuning Efficient tuning using soft prompts, originating in the domain of natural language processing, has gained a lot of attention [19]. This approach has also been applied in the vision-language domain to adapt to downstream tasks. CoOp [48] was the first to apply learnable prompts for CLIP model, replacing manual prompts for each domain. ProDA [26] observes that these text prompts can be viewed as a distribution and proposes prompt distributional learning for higher quality results. CoCoOp [47] conditions text prompts on images to prevent overfitting to base classes. KgCoOp [39] regularizes by minimizing the discrepancy between learned and manual prompts. UPT [43] examines both VPT [15] and text prompts, proposing a unified approach to generate visual and textual prompts from the same architecture. MaPLe [16] employs the alignment of visual and text prompts for improvement with deep prompts, while DCP [25] uses an attention mechanism for this alignment. There is also a line of research aimed at preventing the forgetting of general knowledge. ProGrad [49] aligns gradient directions to preserve general knowledge, and PromptSRC [17] utilizes multiple regularization losses with Gaussian aggregation of model weights to prevent forgetting.

Adapter-style Tuning Adapter-style tuning has been extensively explored as an alternative to prompt tuning. CLIP-Adapter [8] was the first proposed method in this area, utilizing a two-layer MLP structure with ReLU nonlinearity in between. Additionally, it incorporates a residual connection to preserve general knowledge. For improved efficiency, Tip-Adapter [46] employs a cache-based model to save the features and labels of few-shot samples, using them to predict test outcomes without further training. This approach also facilitates better fine-tuning by using the cache as initial training points for further refinement. Differently, Task Residual [42] adopts a unique strategy by simply adding a residual or bias term vector for each class, reducing reliance on pre-trained features. Zhu et al. [50] enhances cache-based models through prior refinement, which involves selecting important features for the cache-based model.